ACERP: Vol. 6, No.2, (Spring 2020) 17-23

Advanced Ceramics Progress

Research Article

Journal Homepage: www.acerp.ir

Studying the Optical Density, Topography, and Structural Properties of CZO and CAZO Thin Films at Different Annealing Temperatures

N. Rahimi [a], V. Dalouji [a *], A. Souri [b]

[a] *Department of Physics, Faculty of Science, Malayer University, Malayer, Iran*
[b] *Department of Materials Engineering, Faculty of Engineering, Malayer University, Malayer, Iran*

PAPER INFO

Paper history:

Received 23 February 2020
Accepted in revised form 23 April 2020

Keywords:

The CAZO Thin Films
Fractal Dimensions
Topography
Optical Density
Bearing Area

ABSTRACT

In this paper, CAZO and CZO thin films were deposited on quartz substrates by radio frequency magnetic sputtering and annealed at different temperatures of 400, 500, and 600°C. One of the most structural studies of thin-film materials is the analysis of the results that are obtained from AFM images. The most variations in optical density of CZO and CAZO thin films were at energy points to about 3eV and 4eV, respectively. Fractal dimensions and structural properties of films, as well as the optical density of CZO and CAZO thin films, were investigated. The AFM images were used to estimate the lateral size of the nanoparticles on the surface of the films. Annealed films at 500°Chad the maximum values for the lateral size of the nanoparticles. These values for the as-deposited films and annealed films at different temperatures of 400, 500, and 600°C were about 7.9,8.1, 6.5, and 7.75nm for CZO thin films, respectively. In addition, the lateral size of CAZO thin films was about 6.8, 6.27, 6.04, and 6.71, respectively. Films that annealed at 500°Chad the minimum value of fractal dimensions. The power spectral density of all films reflects the inverse power low variations, especially in the high spatial frequency region, indicating the presence of fractal components in prominent topographies. The maximum variations in the bearing area were as much as 0.015μm and 0.01μm for CZO thin films and CAZO thin films, respectively.

1. INTRODUCTION

Nowadays, nanomaterials play an important role in different branches of science, such as materials, industry, and chemistry [1-9]. The zinc oxide thin films were applied extensively in optoelectronics, Transparent Conductive Oxide (TCO) films transistors, and biosensors [10,11]. One of the most structural studies of thin-films materials were obtained from AFM images [12]. Extensive efforts have been made to develop the next-generation of optoelectronic devices based on transparent conductive materials that are gaining more attention due to their electrical and optical properties [13]. They are used as appropriate materials for various applications, including light-emitting diodes, solar cells, and gas sensors [14-17]. ZnO is an n-type semiconductor that has been attempted to utilize various elements such as Cr, Co, Ni, M, or Fe in ZnO to improve its electrical properties. CuO [18] and Cu_2O_4 [19, 20] have a thin band of 1.2 and 2.2V, respectively. The ionic atoms (Cu^{+1} and Cu^{+2}) are replaced to Zn^{+2} in CZO thin films, which facilitates the alternatives at the Zn site. The different methods such as sol-gel and Radio Frequency (RF)-magnetron sputtering have been used to obtain Cu-doped ZnO thin films [21,22]. Aluminum doped zinc oxide films were prepared by a variety of techniques such as evaporation [23, 24] metal-organic chemical vapor deposition (MOCVD) [25], RF sputtering [19], Sol-gel [26, 27], heat dissipation [28-30], pulsed laser deposition (PLD) [31], and magnetron sputtering [32-36]. Cu-Al-doped ZnO thin films, which are weak magnetic semiconductors, are good candidates as a source of polar rotations and ferromagnetism generation at room temperature [37]. In the previous report by the researchers of this paper [38], the relation between the fractal dimensions of carbon-nickel films regarding their electrical properties were studied in details.

In this work, the effect of doping content and nanoparticle distribution in CZO and CAZO thin films

* Corresponding Author E-mail: Dalouji@yahoo.com (V. Dalouji)
https://doi.org/10.30501/acp.2020.107466

were studied on optical density, surface topography, and the fractal dimensions of films.

2. EXPERIMENTAL PROCEDURE

In this study, the CZO and CAZO films were deposited on quartz substrates by radio frequency magnetron sputtering at room temperature, and then, they were annealed at 400, 500, and 600ºC in Ar atmosphere. The sputtering gas was Ar and O_2 with the (O_2/O_2 + Ar) ratio of 30%, which remained constant during the operation by employing two rotary and turbo pumps. The base pressure of the sputtering chamber was less than 2×10^{-5}mbar. The working pressure was fixed at 6×10^{-3}mbar. The sputtering power is kept at 125W during the growth of the films. In addition, substrates were cleaned with distilled water to remove any possible impurity, which were placed in ethanol and acetone in the ultrasonic cleaner for 10min. The thickness of CZO and CAZO thin films was about 230±5nm. The values obtained from EDAX analyses (an analytical technique used for the elemental analysis or chemical characterization of a sample) for the ratio of these three metals were 90 to 5% by the weight of zinc to copper and aluminum, respectively. Films were annealed in a furnace by argon flux at three temperatures of 400, 500, and 600°C for 1 hour to consider the effects of annealing on the different properties of thin films. AFM system in the contact mode was used for the study of film surfaces. AFM analysis 2-D surface texture provided a deeper insight into their characteristics and implementation in graphical models and computer simulation. Studying surface roughness of samples at the nanometer scale revealed a fractal structure, which confirmed the relationship between the value of the fractal dimensions and surface roughness parameters. The profile meter was employed to measure the thicknesses of films after deposition processes. The optical spectroscopy properties of films were measured by spectrophotometer in the wavelength range of 200–2500nm. The EDAX system was used to study the content of films.

3. RESULTS AND DISCUSSION

The optical density (D_{opt}) of CZO and CAZO thin films can be obtained from the following equation [39, 40]:

$$D_{opt} = \alpha t \quad (1)$$

Where t is the thickness of the thin films.
The absorption coefficient α of films were obtained from Lambert's relation

$$\alpha = 2.303\ A / t \quad (2)$$

where A is the absorbance of the films.
Fig. 1 (a) and (b) show the electrical density of as-deposited films and films that are annealed at different temperatures 400, 500, and 600ºCfor CZO and CAZO films. The optical density for the CZO thin films is constant between 1 and 3eV, which increase with a steep gradient after 3eV. The optical density for the CZO thin films is constant between 1 and 4eV, which increase with a steep gradient after 4eV. The over 3eV, the optical density of CZO thin films annealed at 500°C have a maximum value. However, the over 4eV, the optical density of as-deposited CAZO thin films have a maximum value. In this work, the thickness is fixed. The size of nanoparticle smoothly increases with increasing annealing temperature up to 400°C. However, the size of nanoparticle has significant changes in the photon energy from 400 to 600°C, and miss an index of optical absorption characterization process, which is theoretically 2 and ½ for the allowed indirect and direct transitions, respectively [10].

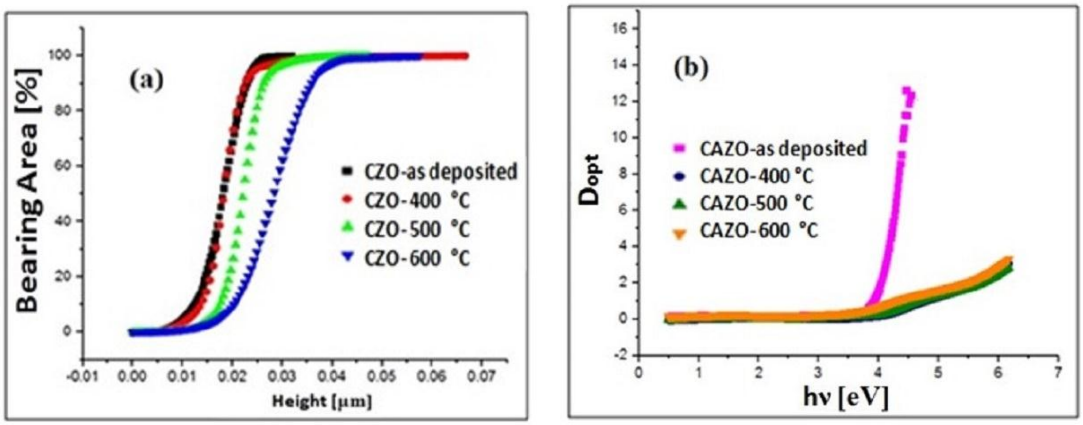

Figure 1. Optical density of as-deposited films and films annealed at 400, 500, and 600°C, (a) CZO and (b) CAZO films

Fig. 2 (a)-(h) show AFM (atomic force microscopy) images of the thin films on the surface of the as-deposited films and films that are annealed at different temperatures 400, 500, and 600°C for CZO and CAZO thin films. Atomic force microscopes (AFM) are a group of scanning probe microscopes that can take biological and non-inductive films in addition to being able to be imaged in a non-vacuum environment. The lateral size of the thin films can be estimated using AFM images. These values for the as-deposited films and films that are annealed at different temperatures400, 500, and 600°C were about 7.9, 8.1, 6.5, and 7.75nm for CZO thin films, respectively. Moreover, the lateral size for CAZO thin films was about 6.8, 6.27, 6.04, and 6.71, respectively. The CZO thin films annealed at 400°C have maximum the amount of nanoparticles lateral size, however the as-deposited CAZO thin films have maximum the amount of nanoparticles lateral size. The AFM images of the CZO films show that nanoparticles are almost spherical and become more amorphous with increasing temperature. However, the CAZO nanoparticles are initially amorphous, spherical, and smaller than the CZO nanoparticles.

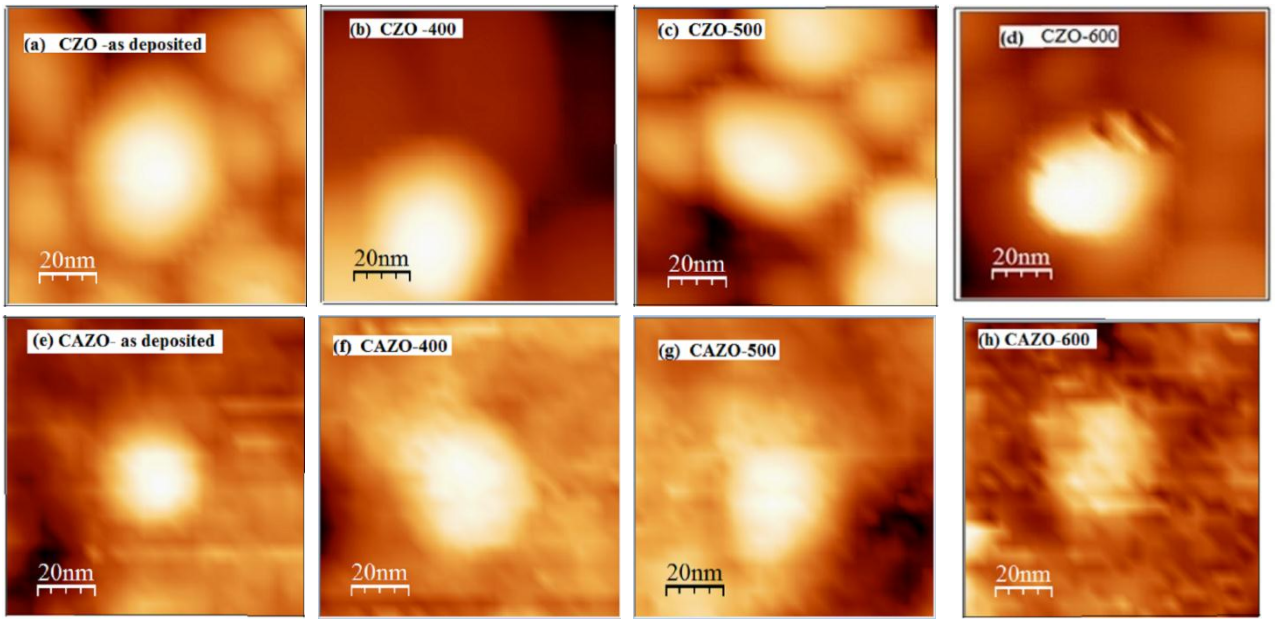

Figure 2. AFM images of nanoparticles on the surface of the CZO and CZAO films for (a,e) the as-deposited films and films that are annealed at different temperatures of (b, f) 400°C, (c, g) 500°C, and (d, h) 600°C

The variation of lateral sizes of film surfaces versus annealing temperature was shown in Fig. 3. It was found that the size of nanoparticles CAZO decreases with the increase in annealing temperature to 500°C, and then, decreases from as-deposited to 500°C. In this way, the CAZO films annealed at 500°C and the CZO at 500°C films have a maximum value of nanoparticles. It can also be seen that the variation of the lateral size of the CZO and CAZO nanoparticles have a slight slope changes. The nanoparticles size changes as Gaussian plots, which can almost be due to little changes in the size of the nanoparticles with the change in temperature. Fig. 4 (a)-(h) show the variation in the height of the thin films on the surface versus the x and z axes for the deposited films and films that are annealed at different temperatures of 400, 500, and 600°C, respectively. The scanning size on the surface of the films was as much as1×1μm by the AFM, the maximum scale value on the x-axis was as much as1μm. The height changes on the

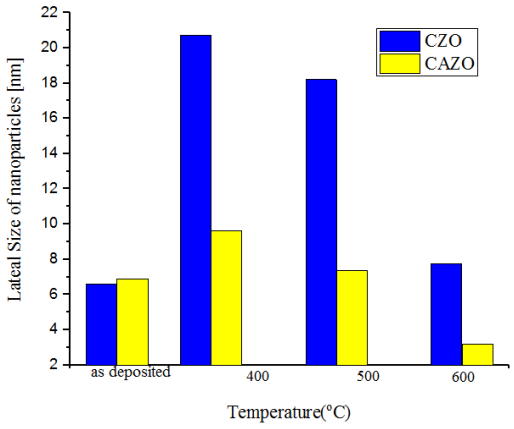

Figure 3. The variations of lateral size of nanoparticles on the surface of the CZO and CZAO thin films for the as-deposited films and films that are annealed at different temperatures of 400, 500, and 600°C

surface of the scanned films show that the films have a topological phase change at 500 and 600°C for CZO thin films and at 600 and 400°C for CAZO thin films. In the deposited films, the *z* values were about 30 and 50nm for the CZO thin films and 9 and 20 nm for CAZO thin films. These results show that the films are smooth in this state, which can have a second phase change. The CAZO nanoparticles have lower fluctuations at room temperature, and the peaks have a slower slope than other temperatures, which have a steep leap above 20nm at 500°C. Also, the CZO nanoparticles at 600°C has lower fluctuations than other temperatures. The *z* ratio of *x* is closely related to both materials, which has many peaks.

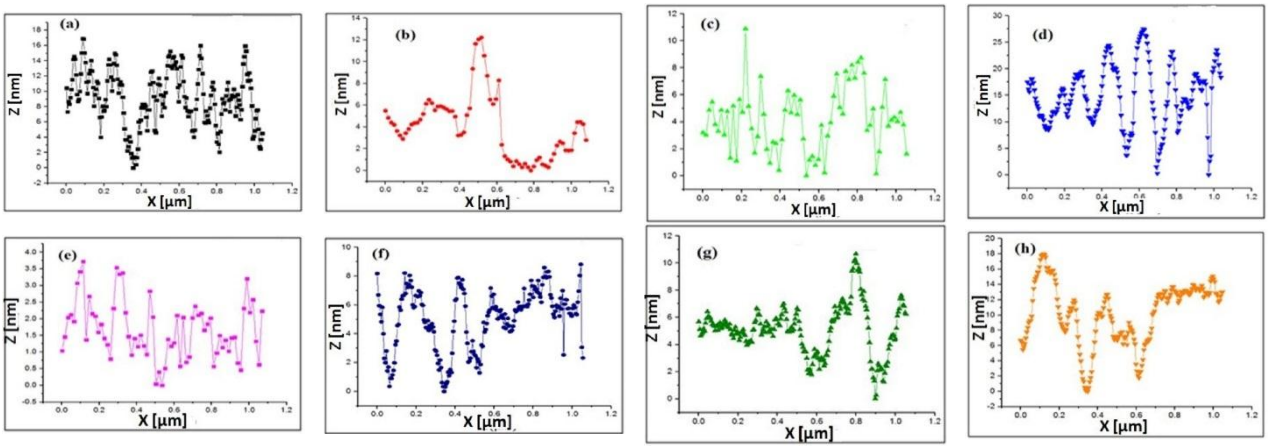

Figure 4. Z-height variations of nanoparticles on the surface of films versus x-axis of the CZO and CZAO thin films for (a,e) the as-deposited films and films that are annealed at different temperatures of (b,f) 400, (c,g) 500, (d,h) 600°C

The PSD spectra were extracted from the scanned area and 1μ×1μ obtained from AFM images of the films as shown in Fig. 2. It can be seen that all the PSD points include a high spatial frequency region. According to the Dynamic Scaling Theory (DST), the power spectral densities (PSDs) analyses closely show how the roughness varies with length scale. The AFM images can be divided into pixels as a small square area where the vectors $h(x_i)$ and $h(y_j)$ are the height at (x_i, y_j) positions. Then, the one-dimensional average of the power spectral densities (PSDs) is given as follows:

$$P(n) = \frac{2L}{N}\left[< \sum_{i=1}^{\frac{N}{2}} (FFT\ (h\ (x_i))^2 >_y + < \sum_{j=1}^{\frac{N}{2}} \left(FFT\ (h\ (y_j)\right)^2 >_x\right] \quad (3)$$

where FFT is the Fast Fourier Transform between the real and reciprocal spaces.

According to the dynamical scaling theory, the relation *P (k)* and frequency *k* are given below for a system with lateral size L [41]

$$\text{P (k)} \propto k^{-\beta} \quad (4)$$

Where β is calculated from the slope of the log-log in PSD spectra of high spatial frequency. The fractal dimensions D_f of films are obtained by solving the β slope of the log-log graph [41]

$$D_f = 4 + {}^{\beta}/_{2} \quad (5)$$

Fig. 5 (a) and 5(b) show the graphs of the spectral density change of the spatial frequency for as-deposited films and films that are annealed at different temperatures of 400, 500, and 600°C. The spectral compaction power of all films reflects the inverse current power variations, especially in the high spatial frequency region, indicating the attendance of fractal components in outstanding topographies. These values determine the relative amounts of surface disorder at different distance scales.

As the annealing temperature increases, the performance of the spectral compaction power increases, which can be due to the decrease in the size of the nanoparticles and have a maximum value at 600°C for CZO films and at 500°C for the CAZO thin films. The values of the fractal dimensions of the films annealed at different annealing temperatures are shown in Fig. 6 that clearly indicates the values of the fractal dimensions depend on the annealing temperature.

The values of the fractal dimensions of the as-deposited CZO thin films and the CZO thin films annealed at 400, 500, and 600°Cwere estimated as much as2.05, 2.07, 2.31, and 2.04, respectively. The values of the fractal dimensions of as-deposited and the CAZO thin films annealed at 400, 500, and 600°C also were estimated as much as2.64, 2.8, 2.9, and 2.7, respectively. Therefore, the fractal dimensions of films increase with the increase of the annealing temperature up to 500°C, and then, decrease over 500°C.

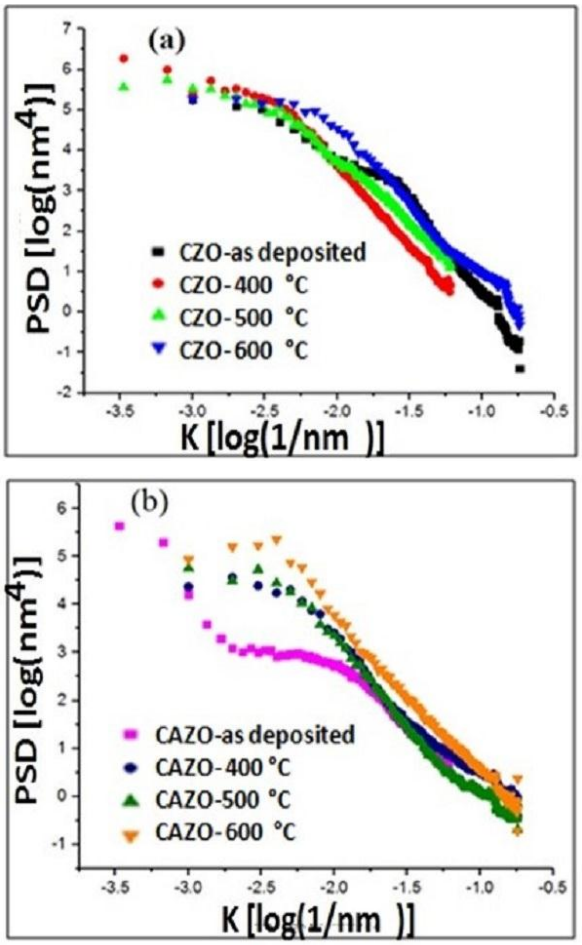

Figure 5. The variations of power spectral density of the films versus frequency k of as-deposited films and annealed films at different temperatures of 400, 500, and 600°C for (a) the CZO thin films and (b) the CAZO thin films

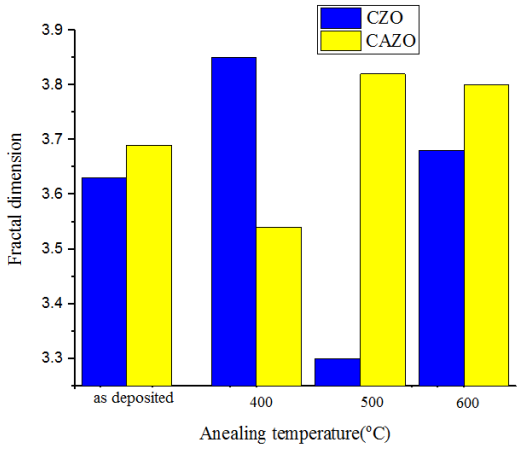

Figure 6. The variationsof fractal dimensions of the CZO thin films and the CAZO thin films annealed at different temperatures of 400, 500, and 600°C

Fig. 7 (a) and (b) show the variations of bearing area of as-deposited CZO and CAZO thin films and CZO and CAZO thin films annealed at400, 500, and 600°C. The CZO thin films in all temperatures have a cavity coverage of less than 10% and layer content of about 95% and 85%, respectively, which are monolayer height. In the vacuum case, the coating is zero, and the content of the films is about 95%, 90% of which is isolated. Furthermore, the cavity coverage is less than 5% for the CAZO thin films as-deposited at room temperature, and the layer content is around 100%, 90% of which is from the height of monolayer. In addition, the monolayer content is over 100% for other temperatures. In the vacuum case, the coating is zero, and the film content is about 100%, 99% of which is isolated.

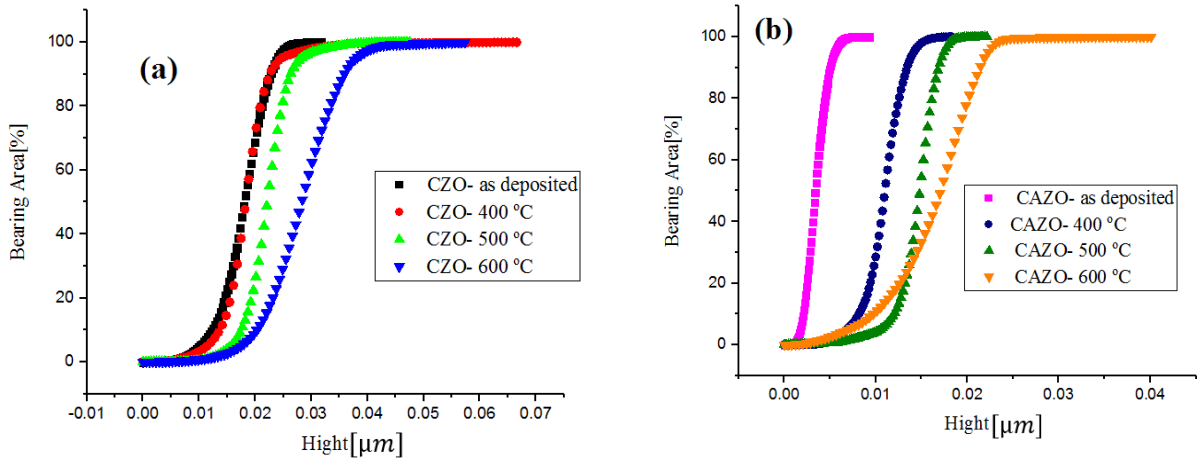

Figure 7. The bearing area of as-deposited films and films that are annealed at different temperatures of 400, 500, and 600°C for (a) CZO films, and (b) CAZO films

4. CONCLUSION

The results suggested that CZO films annealed at 400°C had a maximum lateral size 8.1 nm, and CAZO films annealed at as-deposited had a maximum lateral size as much as 6.8 nm. The CZO and CAZO nanoparticles were almost spherical and became more amorphous with increasing temperature. CZO films showed that nanoparticles were almost spherical and became more amorphous with increasing temperature. However, the CAZO nanoparticles were initially amorphous, spherical, and smaller than the CZO nanoparticles. The CZO and CAZO films had a cavity coverage of less than 10% and 5%, respectively. The optical density had a maximum value both in CZO annealed at 500°C and as-deposited CAZO films. The values of the fractal dimensions of the as-deposited CZO thin films and the CZO thin films annealed at 400, 500, and 600°C were estimated as much as 2.05, 2.07, 2.31, and 2.04, respectively. The values of the fractal dimensions of the as-deposited CAZO thin films annealed at 400, 500, and 600°C also were estimated as much as 2.64, 2.8, 2.9, and 2.7, respectively. It can be seen that the bearing areas of the CZO and CAZO films 600°C had maximum vales and each of them had an increasing function with height.

5. ACKNOWLEDGMENTS

The authors would like to acknowledge the financial support of Malayer University for this research.

REFERENCES

1. Ţălu, Ş., "Micro and nanoscale characterization of three dimensional surfaces: Basics and applications", Napoca Star Publishing House, Cluj-Napoca, Romania, (2015), 350.
2. Dejam, L., Solaymani, S., Achour, A., Stach, S., Ţălu, Ş., Nezafat, N. B., Dalouji, V., Shokri, A. A., Ghaderi, A., "Correlation between surface topography, optical band gaps and crystalline properties of engineered AZO and CAZO thin films", ***Chemical Physics Letters***, Vol. 719, (2019), 78-90.
3. Sobola, D., Ţălu, Ş., Solaymani, S., Grmela, L., "Influence of scanning rate on quality of AFM image: Study of surface statistical metrics", ***Microscopy Research and Technique***, Vol. 80, No. 12, (2017), 1328-1336.
4. Ţălu, Ş., Bramowicz, M., Kulesza, S., Dalouji, V., Solaymani, S., Valedbagi, S., "Fractal features of carbon–nickel composite thin films", ***Microscopy Research & Technique***, Vol. 79, No. 12, (2016), 1208-1213.
5. Stach, S., Sapota, W., Ţălu, Ş., Ahmadpourian, A., Luna, C., Ghobadi, N., Arman, A., Ganji, M., "3-D Surface stereometry studies of sputtered TiN thin films obtained at different substrate temperatures", ***Journal of Materials Science: Materials in Electronics***, Vol. 28, No. 2, (2017), 2113-2122.
6. Zare, M., Solaymani, S., Shafiekhani, A., Kulesza, S., Ţălu, Ş., Bramowicz, M., "Evolution of rough-surface geometry and crystalline structures of aligned TiO_2 nanotubes for photoelectrochemical water splitting", ***Scientific Reports***, Vol. 8, No. 1, (2018), 1-11.
7. Hoseinzadeh, T., Solaymani, S., Kulesza, S., Achour, A., Ghorannevis, Z., Ţălu, Ş., Bramowicz, M., Ghoranneviss, M., Rezaee, S., Boochani, A., Maozaffari, N., "Microstructure, fractal geometry and dye-sensitized solar cells performance of CdS/TiO_2 nanostructures", ***Journal of Electroanalytical Chemistry***, Vol. 830-831, (2018), 80-87.
8. Solaymani, S., Kulesza, S., Ţălu, Ş., Bramowicz, M., Nezafat, N. B., Dalouji, V., Rezaee, S., Karami, H., Malekzadeh, M., Dorbidi, E. S., "The effect of different laser irradiation on rugometric and microtopographic features in zirconia ceramics: Study of surface statistical metrics", ***Journal of Alloys and Compounds***, Vol. 765, (2018), 180-185.
9. Naseri, N., Ţălu, Ş., Kulesza, S., Qarechalloo, S., Achour, A., Bramowicz, M., Ghaderi, A., Solaymani, S., "How morphological surface parameters are correlated with electrocatalytic performance of cobalt-based nanostructures", ***Journal of Industrial and Engineering Chemistry***, Vol. 57, (2018), 97-103.
10. Dejam, L., Solaymani, S., Achour, A., Stach, A., Ţălu, Ş., Nezafat, N. B., Dalouji, V., Shokri, A. A., Ghaderi, A., "Correlation between surface topography, optical band gaps and crystalline properties of engineered AZO and CAZO thin films", ***Chemical Physics Letters***, Vol. 719, (2019), 78-90.
11. Wang, Y., Liu, F., Ji, Y., Yang, M., Liu, W., Wang, W., Sun, Q., Zhang, Z., Zhao, X., Liu, X., "Controllable synthesis of various kinds of copper sulfides (CuS, Cu_7S_4, Cu_9S_5) for high-performance super capacitors", ***Dalton Transactions***, Vol. 44, No. 22, (2015), 10431-10437.
12. Sobola, D., Ţălu, Ş., Solaymani, S., Grmela, L., "Influence of scanning rate on quality of AFM image: Study of surface statistical metrics", ***Microscopy Research and Technique***, Vol. 80, No. 12, (2017), 1328-1336.
13. Dalouji, V., Solaymani, S., Rezaee, S., Mehrparvar**,** D., "Nonmetal—Metal transition in carbon films embedded by Ni nanoparticles: The temperature coefficient of resistivity (TCR), Raman spectra and surface morphology", ***Optik*** ,Vol. 156, (2018), 338-345.
14. Matsumura, M., Camata, R. P., "Pulsed Laser Deposition and Photoluminescence Measurements of ZnO Thin Films on Flexible Polyimide Substrates", ***Thin Solid Films***, Vol. 476, No. 2, (2005), 317-321.
15. Chaabouni, F., Costa, L. C., Abaab, M., Monteiro, J., "Characterization of n-Type: ZnO: Al Films Grown by Magnetron Sputtering", In ***Materials Science Forum*** (Vol. 514-516, 1358-1362), Trans Tech Publications Ltd, Zurich-Uetikon, Switzerland, (2006).
16. Minami, T., Nishi, Y., Miyata, T., "Effect of the thin Ga_2O_3 layer in n^+-ZnO/n-Ga_2O_3/p-Cu_2O heterojunction solar cells"**,** ***Thin Solid Films***, Vol. 549, (2013), 65–69.
17. Casadei, A., Pecora, E. F., Trevino, J., Forestiere, C., Ruffer, D., Russo-Averchi, E., Matteini, F., Tutuncuoglu, G., Heiss, M., Fontcuberta i Morral, A., Dal Negro, L., "Photonic-plasmonic coupling of GaAs single nanowires to optical nano antennas", ***Nano Letters***, Vol. 14, No. 5, (2014), 2271–2278.
18. Kim, T. W., Ha, H. W, Paek, M. J., Hyun, S. H., Choy, J. H., Hwang, S. J., "Unique phase transformation behavior and visible light photocatalytic activity of titanium oxide hybridized with copper oxide", ***Journal of Materials Chemistry***, Vol. 20, No.16, (2010), 3238–3245.
19. Olsen, L. C., Bohara, R. C., Urie, M. W., "Explanation for low-efficiency Cu_2O Schottky-barrier solar cells", ***Applied Physics Letters***, Vol. 34, No. 1, (1979), 47–49.
20. Nakanishi, Y., Miyake, A., Kominami, H., Aoki, T., Hatanaka, Y., Shimaoka, G., "Preparation of ZnO thin films for high-resolution field emission display by electron beam evaporation", ***Applied Surface Science***, Vol. 142, No. 1-4, (1999), 233-236.
21. Ganesh, V., Salem, G. F., Yahia, I. S., Yakuphanoglu, F., "Synthesis, Optical and Photoluminescence Properties of Cu-

Doped Zno Nano-Fibers Thin Films: Nonlinear Optics", ***Journal of Electronic Materials***, Vol. 47, No. 3, (2018), 1798-1805.

22. Zheng, J. H., Song, J. L., Li, X. J., Jiang, Q., Lian, J. S., "Experimental and first-principle investigation of Cu-doped ZnO ferromagnetic powders", ***Crystal Research and Technology***, Vol. 46, No. 11, (2011), 1143-1148.
23. Jin, M., Feng, J., De-Heng, Z., Hong-lei, M., Shu-Ying, L., "Optical and electronic properties of transparent conducting ZnO and ZnO: Al films prepared by evaporating method", ***Thin Solid Films***, Vol. 357, No. 2, (1999), 98-101.
24. Lee, J. H., Chou, C. Y., Bi, Z., Tsai, C. F., Wang, H., "Growth-controlled surface roughness in Al-doped ZnO as transparent conducting oxide", ***Nanotechnology***, Vol. 20, No. 39, (2009), 395704.
25. Zang, Z., Wen, M., Chen, W., Zeng, Y., Zu, Z., Zeng, X., Tang, X., "Strong yellow emission of ZnO hollow nano spheres fabricated using polystyrene spheres as templates", ***Materials & Design***, Vol. 84, (2015), 418–421.
26. Jimenez-Gonzalez, A. E., Urueta J. A. S., Suarez-Parra, R., "Optical and electrical characteristics of aluminum-doped ZnO thin films prepared by sol gel technique", ***Journal of Crystal Growth***, Vol. 192, No. 3-4, (1998), 430-438.
27. Tang, W. Cameron, D. C., "Aluminum-doped zinc oxide transparent conductors deposited by the sol-gel process", ***Thin Solid Films***, Vol. 238, No. 1, (1994), 83-87.
28. Vigil, O., Cruz, F., Santana, G., Vaillant, L., Morales-Acevedo, A., Contreras-Puente, G., "Influence of post-thermal annealing on the properties of sprayed cadmium–zinc oxide thin films", ***Applied Surface Science***, Vol.161, No. 1-2, (2000), 27-34.
29. Nunes, P., Malik, A., Fernandes, B., Fortunato, E., Vilarinho, P., Martins, R., "Influence of the doping and annealing atmosphere on zinc oxide thin films deposited by spray pyrolysis", ***Vacuum***, Vol. 52, No. 1-2, (1999), 45-49.
30. Nunes, P., Fortunato, E., Martins, R., "Influence of the post-treatment on the properties of ZnO thin films", ***Thin Solid Films***, Vol. 383, No. 1-2, (2001), 277-280.
31. Jin, B. J., Woo, H. S., Im, S., Bae, S. H., Lee, S. Y., "Relationship between photoluminescence and electrical properties of ZnO thin films grown by pulsed laser deposition", ***Applied Surface Science***, Vol.169–170, (2001), 521-524.
32. Meng, X. Q., Zhen, W., Guo, J. P., Fan, X. J., "Structural, optical and electrical properties of ZnO and ZnO-Al2O3 films prepared by dc magnetron sputtering", ***Applied Physics A***, Vol. 70, No. 4, (2000), 421–424.
33. Minemoto, T., Negami, T., Nishiwaki, S., Takakura, H., Hamakawa, Y., "Preparation of $Zn_{1-x}Mg_xO$ films by radio frequency magnetron sputtering", ***Thin Solid Films***, Vol. 372, No. 1-2, (2000), 173-176.
34. Minami, T., Sonohara, H., Kakumu, T., Takata, S., "Highly Transparent and Conductive $Zn_2In_2O_5$ Thin Films Prepared by RF Magnetron Sputtering", ***Japanese Journal of Applied Physics***, Vol. 34, No. 8A, (1995), L971.
35. Minami, T., Yamamoto, T., Miyata, T., "Highly transparent and conductive rare earth-doped ZnO thin films prepared by magnetron sputtering", ***Thin Solid Films***, Vol. 366, No. 1-2, (2000), 63-68.
36. Tominaga, K., Kataoka, M., Manabe, H., Ueda, T., Mori, I., "Transparent ZnO: Al films prepared by co-sputtering of ZnO: Al with either a Zn or an Al target", ***Thin Solid Films***, Vol. 290–291, (1996), 84-87.
37. Serin, T., Atilgan, A., Kara, I., Yildiz, A., "Electron transport in Al-Cu co-doped ZnO thin films", ***Journal of Applied Physics***, Vol. 121, No. 9, (2017), 095303.
38. Dalouji, V., "Power spectral densities and polaron hopping conduction parameters in carbon films embedded by nickel nanoparticles", ***Optik***, Vol. 148, (2017), 1-7.
39. Hassanien, A. S., Akl, A. A., "Effect of Se addition on optical and electrical properties of chalcogenide CdSSe thin films", ***Superlattices and Microstructures***, Vol. 89, (2016), 153-169.
40. Van Zeghbroeck, B., "Principles of Electronic Devices", Boulder, University of Colorado, (1997).
41. Raoufi, D., "Fractal analyses of ITO thin films: A study based on power spectral density", ***Physica B: Condensed Matter***, Vol. 405, No. 1, (2010), 451-455.